Surface Estimation Methods with Phased-Arrays for Adaptive Ultrasonic Imaging in Complex Components

S. Robert[a)], P. Calmon, M. Calvo, L. Le Jeune, and E. Iakovleva

CEA- LIST, Centre de Saclay, F-91191, Gif-sur-Yvette cedex, France

[a)]sebastien.robert@cea.fr

Abstract. Immersion ultrasonic testing of structures with complex geometries may be significantly improved by using phased-arrays and specific adaptive algorithms that allow to image flaws under a complex and unknown interface. In this context, this paper presents a comparative study of different Surface Estimation Methods (SEM) available in the CIVA software and used for adaptive imaging. These methods are based either on time-of-flight measurements or on image processing. We also introduce a generalized adaptive method where flaws may be fully imaged with half-skip modes. In this method, both the surface and the back-wall of a complex structure are estimated before imaging flaws.

INTRODUCTION

Ultrasonic immersion testing of structures with irregular geometries can be performed with immersion standard probes coupled with adaptive imaging algorithms [1-3]. Compared to smart flexible contact phased-arrays [4], the manufacturing cost of standard probes is less expansive, which increasingly interests the NDT community.

The general principle of all the adaptive imaging methods in immersion testing can be summarized in two steps: first, the surface is determined by recording and processing the interface echoes; next, the ultrasonic paths through the measured surface are calculated in order to update focusing laws and to preserve the image quality in the structure. This paper deals with the surface measurement step, and present a review of the different Surface Estimation Methods (SEM) available in the CIVA software [5]. These methods are based either on a time-of-flight measurement or on image processing (edge detection, segmentation). A new method based on the Surface Adaptive Ultrasounds (SAUL) technique, originally developed for immersion testing of aeronautical composite structures, is also presented and compared to the others in terms of surface reconstruction speed and accuracy [6]. Finally, we present a generalized adaptive method, based on the Total Focusing Method (TFM) [7-8], where flaws are imaged with half-skip echoes [9]. In this method, the surface and the back-wall of a complex specimen are reconstructed before imaging flaws.

The four SEM algorithms (pulse-echo, pitch-catch, SAUL and TFM methods) are evaluated experimentally for three typical geometries often encountered in NDT applications: the irregular surface of a leveled weld, the concave surface of a nozzle weld junction, and the convex surface of a butt weld. For each geometry type, we compare the measured surfaces, and the effects of surface measurement errors are evaluated on the TFM images of artificial flaws.

41st Annual Review of Progress in Quantitative Nondestructive Evaluation
AIP Conf. Proc. 1650, 1657-1666 (2015); doi: 10.1063/1.4914787

PRINCIPLE OF SURFACE ESTIMATION METHODS

SEM in Pulse-Echo Mode

The first SEM proposed relies on the measurement of the times of flight of the surface echo with a simple electronic scanning (a single element is used at each transmission and the same element is used as receiver). For a phased-array composed of N elements, the number of measured times of flight, denoted by t_m, is $M \leq N$ ($1 \leq m \leq M$) where M depends on the surface complexity. In practice, the time-of-flight measurement is carried out by setting an amplitude threshold above the noise level in water (electronic noise) and by detecting the first maximum (specular echo) of each elementary signal. Thus, the t_m values correspond to the shortest travel times between the elements and the surface, and the impact points P_m to be determined are the intersection points with the perpendicular rays (see Fig. 1).

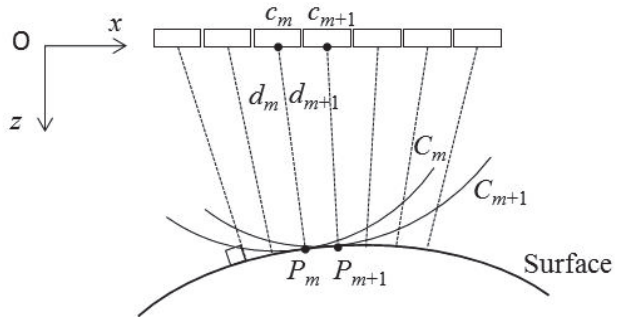

FIGURE 1. A point P_m detected from a simple electronic scanning belongs to a circle C_m of center c_m and radius d_m, where c_m is the center of an element m and d_m is the specular distance to the surface.

A point P_m belongs to a circle C_m of center c_m (element center) and radius d_m, where $d_m = vt_m/2$ is the specular distance between the element m and the surface (v is the sound velocity in water). Assuming that all the echoes arise from specular reflection, the surface can be estimated by the curve tangential to M circles. Then, with the notations in Fig. 1, the coordinates x_m and z_m of a point P_m are given by

$$\begin{cases} x_m = c_m + d_m d'_m \\ z_m = d_m \sqrt{1 - \left(d'_m\right)^2} \end{cases} \tag{1}$$

where

$$d'_m = \frac{d_{m+1} - d_m}{c_{m+1} - c_m}. \tag{2}$$

For M measured times of flight, the reconstructed surface is described by M-1 impact points.

SEM in Pitch-Catch Mode

In case of more complicated surfaces, the robustness of the SEM algorithms may be improved by processing signals recorded in pitch-catch mode, such as the elementary signals of the Full Matrix Capture (FMC) acquisition. If N is the number of elements used both in transmission and reception, the FMC acquisition consists in recording the complete set of NxN inter-element impulse signals $s_{ij}(t)$, where both indexes j and i denote a pair of transmitter and receiver of the array, respectively. As previously, M (with $M \leq N$xN) represents the number of measured times

of flight t_m ($1 \le m \le M$) that mostly depends on the surface complexity. The ray path associated to a measured time of flight t_m is described in below Fig. 2.

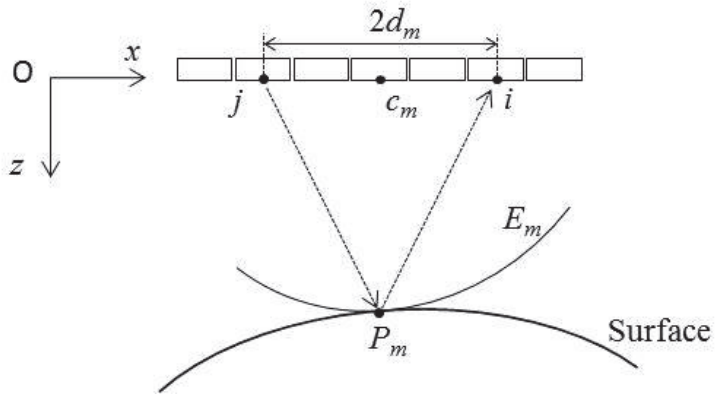

FIGURE 2. A point P_m detected from an inter-element impulse signal $s_{ij}(t)$ belongs to an ellipse E_m whose two foci correspond to the centers of the transmitter j and the receiver i. $a_m = vt_m/2$ and b_m are the major and minor semi-axes of the ellipse E_m.

A time of flight t_m measured from a signal $s_{ij}(t)$ defines a point P_m of the object surface. This point belongs to an ellipse E_n whose foci are the centers of the transmitter j and the receiver i, respectively. The distance $2d_m$ between both the elements j and i is the minor axis of E_n, while $2a_m = vt_m$ corresponds to its major axis. In the pitch-catch mode, the reconstructed surface is the curve tangential a family of M ellipses, which can be calculated as follows:

$$\begin{cases} x_m = c_m + a_m \Delta_m \\ z_m = b_m \sqrt{1 - \Delta_m^2} \end{cases}, \tag{3}$$

where

$$\Delta_m = \frac{-b_m + \sqrt{{b_m}^2 - 4a_m b'_m \left(a_m b'_m - a'_m b_m\right)}}{2\left(a'_m b_m - a_m b'_m\right)}, \tag{4}$$

and

$$a'_m = \frac{a_{m+1} - a_m}{c_{m+1} - c_m}, \tag{5}$$

$$b'_m = \frac{b_{m+1} - b_m}{c_{m+1} - c_m}, \tag{6}$$

$$b_m = \sqrt{a_m^2 - d_m^2}\ . \tag{7}$$

SEM with the SAUL Method

The SAUL method (acronym for Surface Adaptive Ultrasounds) is an adaptive algorithm developed for the inspection of complex composite structures, especially in aerospace. The goal is to transmit in water an incident wave-front that is parallel to the complex surface (normal incidence technique). This is achieved by means of an iterative algorithm that does not require prior knowledge about the geometrical and acoustical properties of the component undergoing inspection. In the context of the inspection of metal parts, the SAUL algorithm may also be applied to estimate the surface geometry with a small number of ultrasonic shots.

Figure 3 hereafter illustrates the principle of the SAUL method for the first iteration. The iterative processing begins with the transmission of a plane wave by simultaneously firing with all the elements (Fig. 3a). The reflected wave is received by the phased-array and the times of flight between all the elements and the surface are measured (Fig. 3b). Then, a delay law is calculated from these measured times of flight and applied to a second ultrasonic shot (Fig. 3c). Depending on the geometry complexity, the process is iterated as many times as necessary to converge and to obtain an incident wave-front rigorously parallel to the surface.

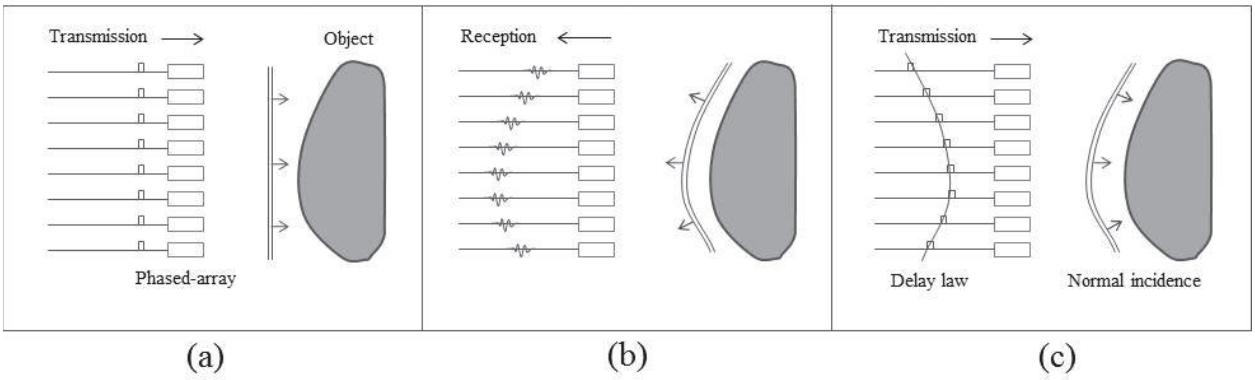

FIGURE 3. Three steps of first SAUL iteration: a plane wave is transmitted by firing with the full array (a); the reflected wave is received by the array and times of flight are measured (b); a delay law is deduced from these measurements and applied to obtain an incident wave-front parallel to the object surface (c).

Mathematically, if M is the number of measured times of flight in the SAUL method ($M \leq N$ where N is the total number of elements), the transmission and reception delays applied to an element m ($1 \leq m \leq M$) are defined as:

$$E_m^{(j+1)} = E_m^{(j)} - \frac{t_m^{(j)}}{2} - \underset{k:1\to M}{\mathrm{Min}}\left(E_k^{(j)} - \frac{t_k^{(j)}}{2} \right), \tag{8}$$

$$R_m^{(j+1)} = \underset{k:1\to M}{\mathrm{Max}}\left(E_k^{(j)} - \frac{t_k^{(j)}}{2} \right) - E_m^{(j)} + \frac{t_m^{(j)}}{2}, \tag{9}$$

where j (j = 1, 2,…) denotes the shot number in the iterative processing (j = 1 corresponds to the first transmission without delay law, i.e. $E_m^{(1)} = 0 \; \forall m$), and $t_m^{(j)}$ is the measured time of flight for an element m and a shot j. Equations (8) and (9) express a summation of delay laws, iteration after iteration, until the convergence is satisfactory. In general, this is achieved after no more than four or five ultrasonic shots.

At the SAUL convergence, it is possible to obtain the specular times of flight that would have been measured with a simple electronic scanning, i.e. with N shots (such as in the SEM algorithm in pulse echo). Let E_m and t_m denote the transmission delay and the time of flight for an element m when the algorithm has converged, the corresponding specular time of flight t_m' can be calculated as follows:

$$t_m' = t_m - 2E_m + \underset{k:1\to M}{\mathrm{Max}}(E_k). \tag{10}$$

Next, the surface geometry is estimated by calculating the curve tangential to M circles, as in the electronic scanning method. This is the second interesting application of the SAUL method since, contrary to the SEM algorithm in pulse-echo mode, the speed of surface reconstruction does not depend on the number of elements anymore (N shots for N elements), but on the number of iterations (four or five shots).

SEM by TFM Imaging

The fourth SEM algorithm available in CIVA is based on the TFM (Total Focusing Method) imaging technique. The TFM imaging is a coherent summation of the *N*x*N* inter-element impulse signals $s_{ij}(t)$ in every point/pixel of an area of interest. Here, we evaluate the amplitude of a point *P* of the TFM image by calculating:

$$A(P) = \left| \sum_{i=1}^{N} \sum_{j=1}^{N} s_{ij}\left(t_i^P + t_j^P\right) + jh\left[s_{ij}\left(t_i^P + t_j^P\right) \right] \right|, \tag{11}$$

where t_j^P (resp. t_j^P) is the time of flight between a transmitter *j* (resp. receiver *i*) and *P*, and the operator *h* denotes the Hilbert transform.

The principle consists of the SEM consists in imaging the surface considering the ultrasound propagation in water. Then, the surface geometry is extracted from the TFM image with edge detection or segmentation tools. Figure 4 shows an example of surface reconstruction with the TFM imaging. A second TFM image can be then displayed in the solid by processing the same set of experimental data and by considering the ultrasound propagation through the complex water/solid interface. This two-steps adaptive TFM imaging has been recently implemented in real-time ultrasonic systems [1-2].

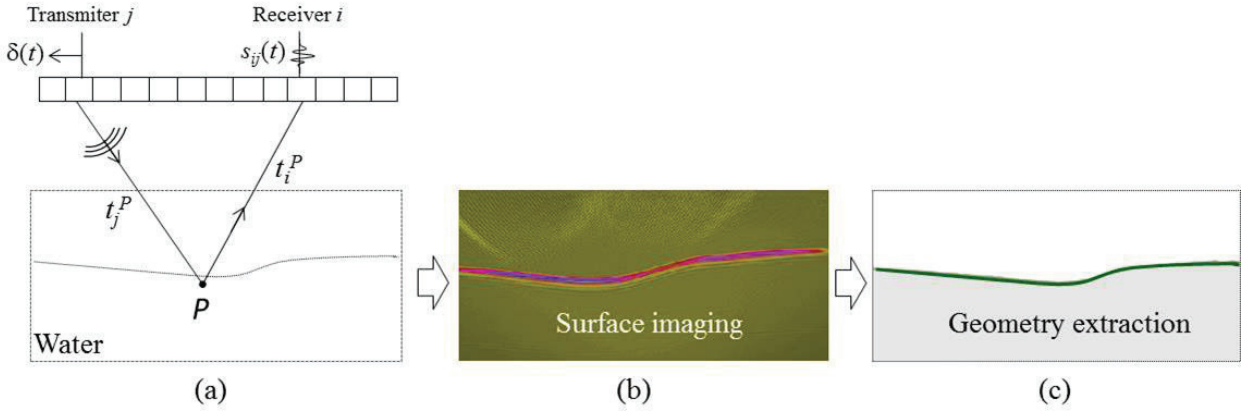

FIGURE 4. Principle of the surface estimation method with the TFM imaging: focusing of the inter-element signals $s_{ij}(t)$ on a point *P* by assuming a water medium in the time-of-flight calculation model (a), surface image (b), extracted geometry (c).

EVALUATION OF THE METHODS: APPLICATION TO FLAW IMAGING

The SEM algorithms have been evaluated with three steel mock-ups of different geometry types (see Fig. 5). They correspond to complex shapes often encountered in ultrasonic NDT: an irregular geometry representative of a leveled weld; a concave surface (curvature radius of 100 mm) of a nozzle weld junction; a convex surface (curvature radius of 80 mm) of a butt weld. The same phased-array is used throughout the evaluation: 64 elements, 0.8 mm pitch and 2 MHz central frequency. For each specimen, it is positioned approximately at 20 mm from the surface.

In the following, the robustness of the different methods is evaluated by comparing the reconstructed geometries with the real one (provided by the manufacturer) and by comparing the quality of the TFM images of the defects inside the part. The location and dimensions of the TFM areas are indicated in Fig. 5.

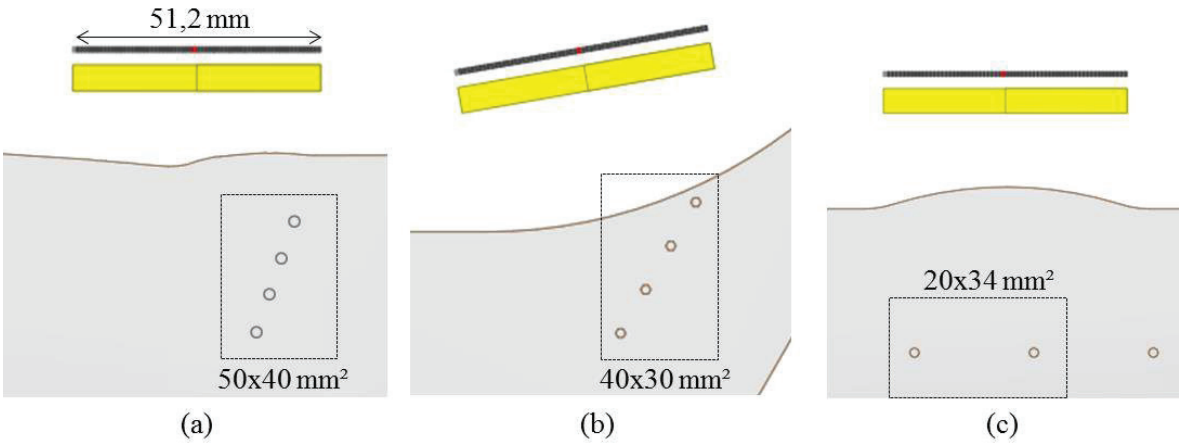

FIGURE 5. Steel mock-ups with different surface geometries: irregular geometry of a leveled weld (a), concave surface representative of a nozzle junction (b), convex surface of a butt weld (c). In each case, holes of 2 mm diameter are located under the complex surface, and the TFM area (location and dimensions) is described.

The geometries obtained with the four SEM algorithms are superimposed in Fig. 6 and can be compared with the nominal profile provided by the manufacturer. It can be noticed that the profiles are in excellent agreement for the concave (Fig. 6b) and convex surfaces (Fig. 6c). The maximum error between the reconstructed profiles and the nominal one is less than 0.05 mm, which represents $\lambda/15$ in terms of wavelength in water (at 2 MHz). The example of the leveled weld (Fig. 6a) shows that the SEM algorithms in pulse-echo mode and with the SAUL method are less robust, in the case of small concavity. The maximum errors are 0.20 mm ($\lambda/4$) for the pulse-echo mode and 0.35 mm ($\lambda/2$) for the SAUL method around x = 165 mm (the local curvature radius is around 20 mm). The two other methods (pitch-catch and TFM) provide profiles that are more in agreement with the theoretical one (maximum error less than 0.10 mm). This is due to the higher number of processed signals providing, therefore, more information about the surface geometry.

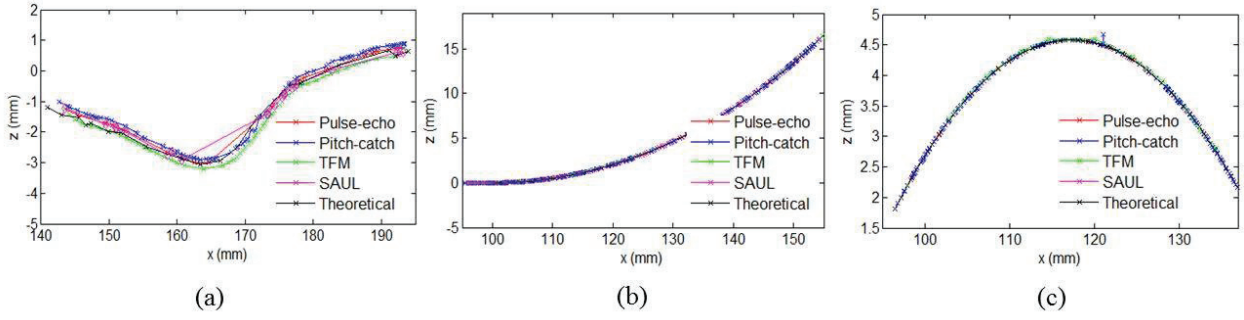

FIGURE 6. Comparison of the 4 measured profiles (pulse-echo in red, pitch-catch in blue, TFM in green, SAUL in magenta) with the theoretical one (black curve) for three specimens: leveled weld (a); nozzle junction (b); butt weld (c).

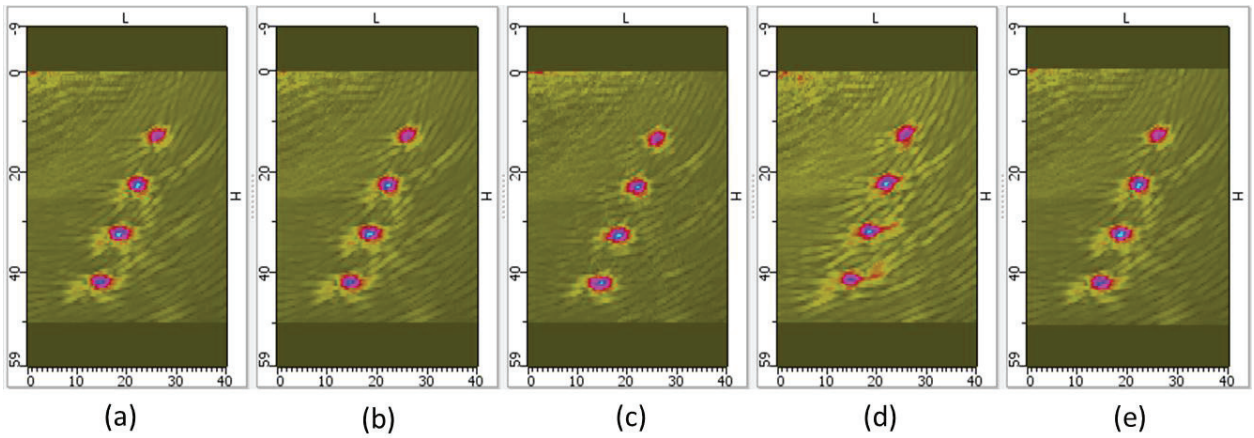

FIGURE 7. TFM imaging of flaws for the leveled weld surface: theoretical surface (a), surfaces estimated in pulse-echo (b), in pitch-catch (c), with SAUL (d), with TFM (e).

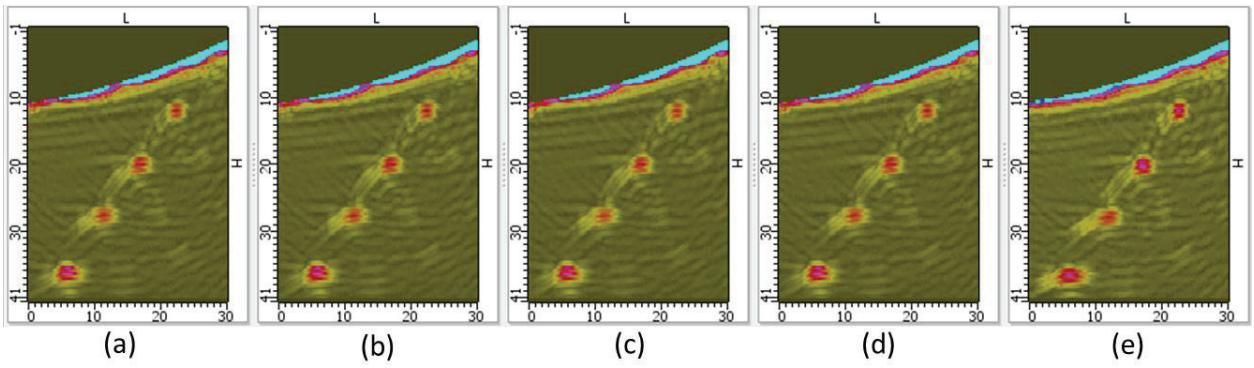

FIGURE 8. TFM imaging of flaws for the nozzle weld surface: theoretical surface (a), surfaces estimated in pulse-echo (b), in pitch-catch (c), with SAUL (d), with TFM (e).

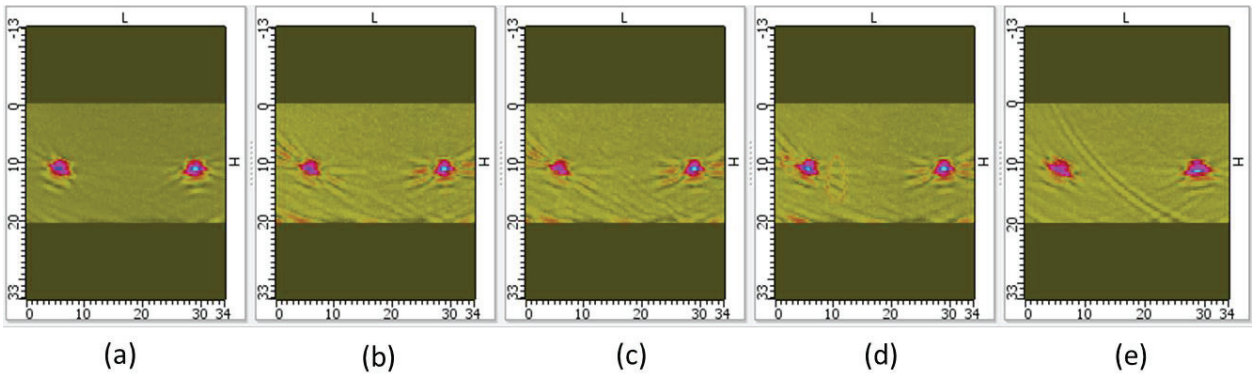

FIGURE 9. TFM imaging of flaws for the butt weld surface: theoretical surface (a) surfaces estimated in pulse-echo (b), in pitch-catch (c), with SAUL (d), with TFM (e).

The TFM images of the reflectors inside the three parts (side drilled holes of 2 mm diameter) accounting for the different profiles (the four profiles obtained from SEM and the nominal one) are displayed in Figs. 7 to 9: Fig. 7 for the leveled weld, Fig. 8 for the nozzle weld, and Fig. 9 for the butt weld. These results are in accordance with the comparisons of profiles in Fig. 6. The SEM algorithms provide almost equivalent results for the nozzle weld and the butt weld, but this is not the case for the irregular leveled weld. The profile obtained with the SAUL method (Fig. 7d) gives an image of lower quality compared to the others (signal-to-noise ratio reduced of 4 dB), which is in agreement with the reconstruction error of 0.35 mm ($\lambda/2$) measured in Fig. 6. The reconstruction error in pulse-echo is twice smaller ($\lambda/4$) and it does not affect the TFM image quality (Fig. 7b).

FULL ADAPTIVE TFM IMAGING ACCOUNTING FOR BOTH SURFACE AND BACK-WALL PROFILES

The main application of full adaptive TFM imaging is to image crack-type flaws with half-skip echoes (echoes involving a reflection at the back-wall) when both the surface and the bottom geometries are not known with accuracy. The final TFM image of cracks is obtained in three steps: 1) reconstruction of the surface profile as described in the previous section; 2) in the same way reconstruction of the back-wall profile from a TFM image taking into account the surface profile; and 3) TFM image of the part taking into account both the surface and back-wall profiles previously reconstructed. The principle of the full adaptive TFM imaging is illustrated in Fig. 10 with a steel mock-up representative of a butt weld. A breaking vertical notch of 10 mm height is located under the complex surface (Fig. 10c). The phased-array (128 elements with 0.6 mm pitch and 5 MHz central frequency) is positioned approximately at 30 mm from the surface.

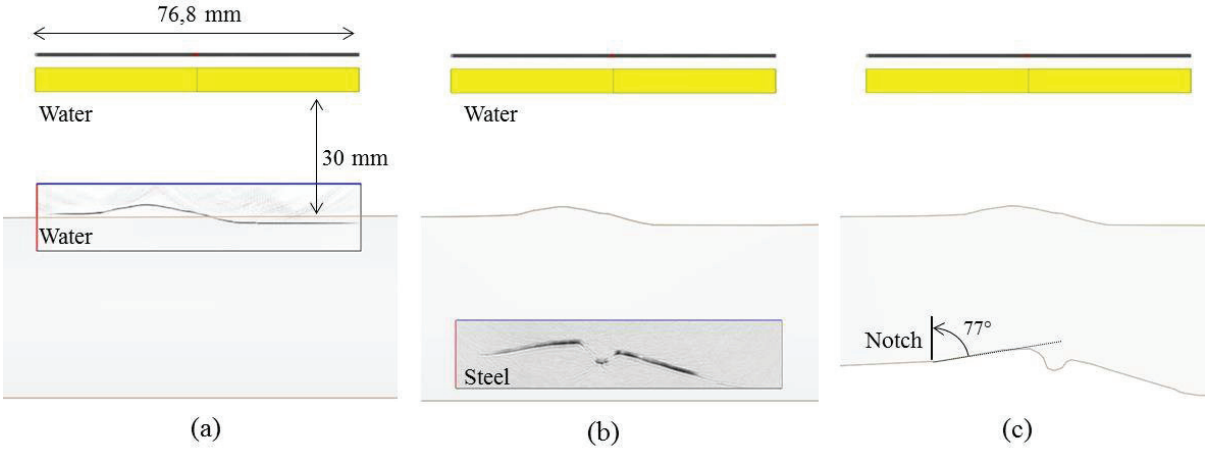

FIGURE 10. Principle of the full adaptive TFM applied to a specimen with a butt weld geometry: surface imaging (a) extraction of the surface geometry and back-wall imaging (b), complete 2D geometry of the butt weld (c).

The back-wall profile is obtained by applying TFM algorithm with times of flight associated to longitudinal (*L*) waves and direct paths. Once the profiles have been estimated, the notch can be fully imaged by considering one of the various possible half-skip echoes. In the present case where the vertical notch forms an angle of 77° with the back-wall around the weld root (Fig. 10c), the optimal imaging half-skip mode corresponds to a *LTT* path ('*T*' denotes a transverse wave), the mode conversion *LT* arising on the back-wall before to intercept the flaw. Figs. 11a and 11b presents, respectively, the *LTT* images calculated respectively with the nominal and reconstructed profiles. We can notice that the notch is better defined with the reconstructed profile than with the nominal one and that the signal-to noise ratio is increased. This is probably due to a slight inaccuracy in the probe position relatively to the nominal profile. The enhanced image quality in Fig. 11b fully demonstrates the usefulness of adaptive imaging methods even if the profile is known since it avoids any problem of probe positioning. It is important to notice that, in adaptive TFM imaging, only a sub-set of elements is needed to image the notch, while the surface estimation uses

the full array. In the present application, both the surface and the back-wall of the butt weld are imaged with 128 elements, but only 64 central elements are used to obtain the final image.

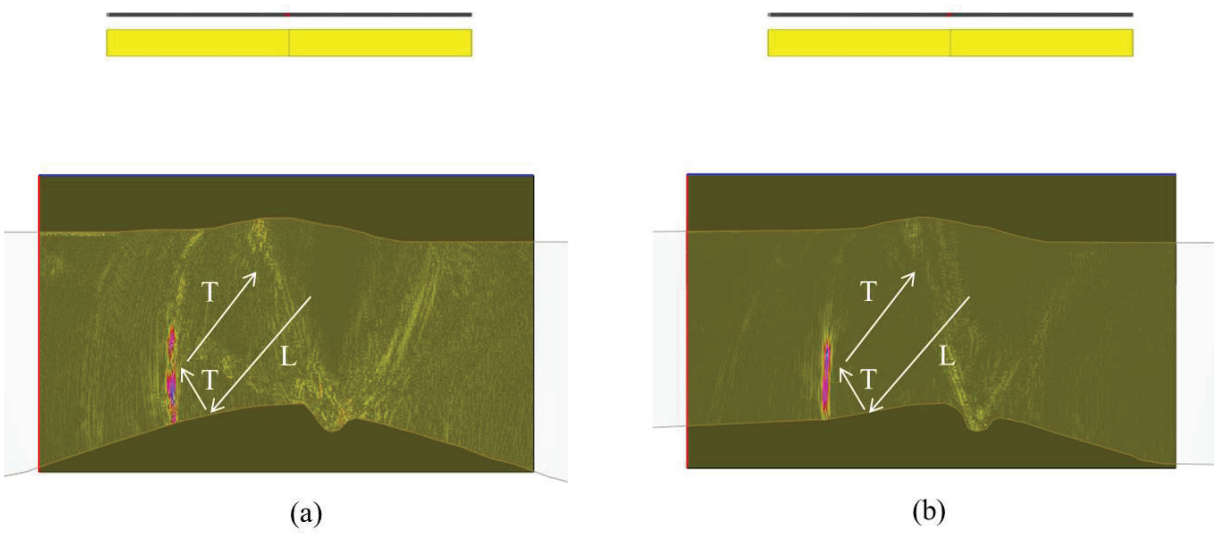

FIGURE 11. TFM imaging of a notch with the *LTT* half-skip mode in a complex mock-up representative of a butt weld: image obtained with the theoretical geometry (a) new enhanced image by applying the full adaptive TFM principle (b).

CONCLUSIONS

In this paper, we have presented the surface estimations methods available in the CIVA software and used for immersion testing of complex shape structures with phased-arrays. The choice of one of these methods for real-time inspections mainly depends on the characteristics of the embedded electronic in multi-channel systems, and on the tradeoff between speed and accuracy. The surface estimation method with the SAUL algorithm is the simplest and fastest one, and it is very promising for surfaces with smooth irregularities. For more complicated surfaces, the method based on the TFM imaging is the most accurate. In addition, we have shown that it is possible to measure the complete 2D geometry (surface and back-wall) of a complex specimen, which allows to image crack-type defects with half-skip modes to improve their characterization [10].

The adaptive TFM imaging has been recently implemented in a prototype ultrasonic system, manufactured by the M2M society. The imaging frame rate is 10 fps and current works are in progress to improve this performance.

REFERENCES

1. D. I. A. Lines, J. Wharrie, and J. Hottenroth,"Real-time full matrix capture + total focusing and other novel imaging options using general purpose PC-based array instrumentation," *Insight - Non-Destructive Testing and Condition Monitoring*, **54**(2), 86-90 (2012).
2. M. Sutcliffe, M. Weston, B. Dutton, P. Charlton, and K. Donne, "Real-Time Full Matrix Capture for Ultrasonic Non-destructive Testing with Acceleration of Post-processing Through Graphic Hardware," *NDT&E International*, **51**, 16-23 (2012).
3. J. Camacho, J. Cruza, J. Brizuela and C. Fritsch, "Automatic Dynamic Depth Focusing for NDT," *IEEE Trans. Ultrason. Ferr. Freq. Control*, **61**(4), 673–684 (2014).
4. O. Casula, C. Poidevin and G. Gattiaux, "Control of Complex Components with Smarts Flexible Phased Arrays," *Ultrasonics*, **44**, 647-651 (2005).

5. More details may be found at http://www-civa.cea.fr and http://www.extende.com/
6. S. Robert, O. Casula, O. Roy, and G. Neau, "Real-time Non-Destructive Testing of Composite Aeronautical Structures with a Self-adaptive Ultrasonic Technique," *Meas. Sci. Technol.*, **24**(7), 2013.
7. L. F. Nock and G. E. Trahey, "Synthetic Receive Aperture Imaging with Phase Correction for Motion and for Tissue Inhomogeneities - Part I: Basic Principles," *Ultrason. Ferr. Freq. Control*, **39**(4), 489–495 (1992).
8. R. Chiao, L. Thomas, and S. Silverstein, "Sparse Array Imaging with Spatially-encoded Transmits," 1997 IEEE Ultrasonics Symposium, *IEEE proceedings*, **2**, 1679–1682 (1997).
9. E. Iakovleva, S. Chatillon, P. Brédif, and S. Mahaut, "Multi-mode TFM imaging with artifacts filtering using CIVA UT forwards models", *Review of Progress in Quantitative Nondestructive Evaluation*, eds. D. E. Chimenti and L. J. Bond, (American Institute of Physics 1581, Melville, NY), **33**, 72-79 (2014).
10. L. Le Jeune, S. Robert, P. Dumas, A. Membre, and C. Prada, "Adaptive Ultrasonic Imaging with the Total Focusing Method for Inspection of Complex Components Immersed in Water," *Review of Progress in Quantitative Nondestructive Evaluation*, eds. D. E. Chimenti and L. J. Bond, July 20–25 July 2014, Boise, Idaho, USA.